
The Effect of Including Bone in Dixon-Based Attenuation Correction for ^{18}F -Fluciclovine PET/MRI of Prostate Cancer

Mattijs Elschot¹, Kirsten M. Selnæs^{1,2}, Håkon Johansen^{1,3}, Brage Krüger-Stokke^{1,4}, Helena Bertilsson^{5,6}, and Tone F. Bathen^{1,2}

¹Department of Circulation and Medical Imaging, Norwegian University of Science and Technology, Trondheim, Norway; ²St. Olavs Hospital, Trondheim, Norway; ³Department of Nuclear Medicine, St. Olavs Hospital, Trondheim, Norway; ⁴Department of Radiology, St. Olavs Hospital, Trondheim, Norway; ⁵Department of Urology, St. Olavs Hospital, Trondheim, Norway; and ⁶Department of Cancer Research and Molecular Medicine, Norwegian University of Science and Technology, Trondheim, Norway

The objective of this study was to evaluate the effect of including bone in Dixon-based attenuation correction for ^{18}F -fluciclovine PET/MRI of primary and recurrent prostate cancer. **Methods:** ^{18}F -fluciclovine PET data from 2 PET/MRI studies—one for staging of high-risk prostate cancer (28 patients) and one for diagnosis of recurrent prostate cancer (81 patients)—were reconstructed with a 4-compartment (reference) and 5-compartment attenuation map. In the latter, continuous linear attenuation coefficients for bone were included by coregistration with an atlas. The SUV_{max} and mean 50% isocontour SUV (SUV_{iso}) of primary, locally recurrent, and metastatic lesions were compared between the 2 reconstruction methods using linear mixed-effects models. In addition, mean SUVs were obtained from bone marrow in the third lumbar vertebra (L3) to investigate the effect of including bone attenuation on lesion-to-bone marrow SUV ratios (SUVR_{max} and SUVR_{iso} ; recurrence study only). The 5-compartment attenuation maps were visually compared with the in-phase Dixon MR images for evaluation of bone registration errors near the lesions. *P* values of less than 0.05 were considered significant. **Results:** Sixty-two lesions from 39 patients were evaluated. Bone registration errors were found near 19 (31%) of these lesions. In the remaining 8 primary prostate tumors, 7 locally recurrent lesions, and 28 lymph node metastases without bone registration errors, use of the 5-compartment attenuation map was associated with small but significant increases in SUV_{max} (2.5%; 95% confidence interval [CI], 2.0%–3.0%; *P* < 0.001) and SUV_{iso} (2.5%; 95% CI, 1.9%–3.0%; *P* < 0.001), but not SUVR_{max} (0.2%; 95% CI, –0.5%–0.9%; *P* = 0.604) and SUVR_{iso} (0.2%; 95% CI –0.6%–1.0%; *P* = 0.581), in comparison to the 4-compartment attenuation map.

Conclusion: The investigated method for atlas-based inclusion of bone in ^{18}F -fluciclovine PET/MRI attenuation correction has only a small effect on the SUVs of soft-tissue prostate cancer lesions, and no effect on their lesion-to-bone marrow SUVs when using signal from L3 as a reference. The attenuation maps should always be checked for registration artifacts for lesions in or close to the bones.

Key Words: PET/MRI; attenuation correction; prostate cancer; fluciclovine; FACBC

J Nucl Med 2018; 59:1913–1917

DOI: 10.2967/jnumed.118.208868

Medical imaging plays an increasingly important role in the management of prostate cancer, which is the most frequently detected type of cancer in men in developed countries (1). Multiparametric MRI, that is, the combination of anatomic T2-weighted imaging and functional diffusion-weighted and dynamic contrast-enhanced imaging, is currently recommended for staging of primary prostate cancer (2), whereas molecular imaging with PET has shown promise for the detection of primary and recurrent prostate cancer (3–7). Since the introduction of integrated PET/MRI scanners, these complementary datasets can be simultaneously acquired, thereby potentially improving the diagnostic accuracy in comparison to either modality alone (3,4,8,9).

In contrast to CT, however, MRI does not provide an estimate of the electron densities that determine the attenuation of the 511-keV annihilation photons in the patient's body. Correction for attenuation, which is required for quantitatively accurate PET imaging, is therefore technically challenging on a PET/MRI system. In current clinical practice, fast T1-weighted or Dixon MR scans are used to create an attenuation map with fixed linear attenuation coefficients for 3 (soft tissue, lung, background air) (10) or 4 (soft tissue, fat, lung, and background air) segmented compartments (11), respectively. In both cases, the linear attenuation coefficient of soft tissue is assigned to bones, typically leading to an underestimation of the SUVs in lesions in and near bony structures (12,13). In a simulation study with known ground truth, Keereman et al. estimated the underestimation of SUVs in the prostate region to be around 4% (13).

Paulus et al. recently presented a method to solve this issue, by including continuous bone linear attenuation coefficients in the Dixon-based attenuation map, based on coregistration of the Dixon images with an atlas of MR and CT pairs of the major bones in the body (14). This method, which is currently implemented on Siemens mMR PET/MRI scanners, was reported to substantially reduce the underestimation of SUV in bone lesions (14,15) and soft-tissue lesions in the brain (16). The effect on the SUV in soft-tissue lesions in the body, on the other hand, was particularly small (14,15). However, the latter results were derived from PET/MRI data with ^{18}F -FDG, a radiotracer that is not useful in the context of prostate cancer. Consequently, the effect of model-based inclusion of bone attenuation values has not been assessed for clinical prostate cancer imaging. Incorrect bone attenuation values could affect the quantitative accuracy of prostate (bed), lymph node, and bone lesion SUVs in the bone-dense pelvis, as well as obscure the qualitative comparison with uptake in spinal bone marrow, which is a commonly used evaluation criterion in clinical practice (17).

Received Jan. 26, 2018; revision accepted Apr. 24, 2018.

For correspondence or reprints contact: Mattijs Elschot, Norwegian University of Science and Technology, Mail MTF5*3.1310, P.O. Box 8905, N-7491 Trondheim, Norway.

E-mail: mattijs.elschot@ntnu.no

Published online May 4, 2018.

COPYRIGHT © 2018 by the Society of Nuclear Medicine and Molecular Imaging.

The objective of this work was therefore to investigate the effect of including bone in Dixon-based attenuation correction for PET/MRI of primary and recurrent prostate cancer. For this purpose, we retrospectively analyzed a cohort of patients examined with ^{18}F -fluciclovine (anti-1-amino-3- ^{18}F -fluorocyclobutane-1-carboxylic acid) PET/MRI, which is a Food and Drug Administration- and European Medicines Agency-approved radiotracer for use in recurrent prostate cancer.

MATERIALS AND METHODS

Patients

In this work, we retrospectively reconstructed and analyzed ^{18}F -fluciclovine PET/MRI data from 2 prospective studies performed at our institution (St. Olavs Hospital, Trondheim University Hospital). The first study, which will be referred to as the staging study, included patients classified as high-risk according to modified D'Amico criteria (prostate-specific antigen > 20 ng/mL or clinical stage \geq cT3a or Gleason score \geq 8) to investigate the merit of combined ^{18}F -fluciclovine PET/MRI for locoregional staging of primary prostate cancer (ClinicalTrials.gov; identifier NCT02076503) (18). The second study, which will be referred to as the recurrence study, included patients that fulfilled the European Association of Urology criteria for biochemical relapse after radical treatment (2 consecutive measurements with prostate-specific antigen \geq 0.2 ng/mL after radical prostatectomy or prostate-specific antigen \geq 2.0 ng/mL above the nadir after definitive radiotherapy) to investigate the diagnostic accuracy of combined ^{18}F -fluciclovine PET/MRI for detection of recurrent prostate cancer (ClinicalTrials.gov; identifier NCT02562131). Both studies were approved by our institution and the Regional Committee for Medical and Health Research Ethics Central Norway. All patients gave written informed consent before enrollment.

Imaging and Reconstruction

Both imaging studies were performed on a 3-T Biograph mMR PET/MRI scanner (Siemens Healthcare GmbH). All PET images were offline reconstructed (Siemens HDPET, 3 iterations, 21 subsets, gaussian filter of 4 mm in full width at half maximum) using 4-compartment (soft tissue, fat, lung, and background air) and 5-compartment (soft tissue, fat, lung, background air, and bone) attenuation maps. Both attenuation maps were created from the Dixon MR series (first echo time, 1.23 ms; second echo time, 2.46 ms; repetition time, 3.6 ms; voxel size, $4.1 \times 2.6 \times 3.1$ mm; field of view, $500 \times 329 \times 400$ mm) using the dedicated tool for offline generation of attenuation maps available on the software platform (*synngo* MR E11P; Siemens Healthcare GmbH) of the scanner. In short, for the 4-compartment attenuation map, soft tissue, fat, lung, and air voxels were automatically segmented and assigned fixed 511-keV linear attenuation coefficients of 0.1000, 0.0854, 0.0224, and 0 cm^{-1} , respectively. For the 5-compartment attenuation map, continuous bone linear attenuation coefficients were superimposed on the 4-compartment attenuation map by coregistration of the Dixon series to an atlas of MR and CT pairs of the major bones in the body, as described in more detail by Paulus et al. (14).

In the staging study, the PET images for evaluation of lymph node metastases covered the lymph nodes from the pelvic floor up to the ureteral crossing of the common iliac vessels, as previously described (8,19), and were reconstructed from the counts in a time-window 5–10 min after tracer injection. The PET images for evaluation of prostate tumors were centered on the prostate and were reconstructed from the counts in a time window 33–38 min after tracer-injection. In the recurrence study, PET images were acquired in 4 consecutive, partly overlapping, bed positions covering the patient from the lower pelvis to the neck. Acquisition lasted 4 min per bed position and was started approximately 5 min after tracer injection.

Volumes of Interest (VOIs)

For the patients in the staging study, VOIs of primary prostate tumors and pelvic lymph node metastases were considered. The prostate tumor VOIs were defined as the 50% isocontour of the SUV_{max} in the corresponding histology-based VOIs, which were available from a previous study (19). The lymph nodes classified as malignant by a nuclear medicine physician were retrospectively identified on the PET images reconstructed with the 4-compartment attenuation map. VOIs were defined as the 50% isocontour of the SUV_{max} in a sphere encompassing the entire lymph node. The latter approach was also used to define the VOIs of recurrent prostate tumors, pelvic lymph nodes, paraortic lymph nodes, and bone lesions in the recurrence study. In all cases, isocontouring was performed separately on the PET images reconstructed with the 4 and 5-compartment attenuation maps. In addition, spheric VOIs (8 mm radius) were placed in the third lumbar vertebra (L3) of the patients in the recurrence study to calculate lesion-to-bone marrow SUV ratios (SUVRs).

The SUV_{max} and mean 50% isocontour SUV (SUV_{iso}) were obtained for each of the lesion VOIs. For the patients in the recurrence study, the mean SUVs of the bone marrow VOI (SUV^{bm}) were obtained and maximum and mean lesion-to-bone marrow SUVs were calculated as $\text{SUVR}_{\text{max}} = \text{SUV}_{\text{max}}/\text{SUV}^{\text{bm}}$ and $\text{SUVR}_{\text{iso}} = \text{SUV}_{\text{iso}}/\text{SUV}^{\text{bm}}$, respectively. Bone marrow SUVs were not evaluated for the patients in the staging study because the software did not include the vertebral column in the 5-compartment attenuation maps of these single-bed-position, pelvic datasets. All SUVs and SUVs were obtained separately from the PET images reconstructed with the 4 and 5-compartment attenuation maps. For each VOI, the relative change in SUV was calculated as $\Delta\text{SUV} = (5\text{-compartment SUV}/4\text{-compartment SUV} - 1) \times 100\%$, and the relative change in SUVR as $\Delta\text{SUVR} = (5\text{-compartment SUVR}/4\text{-compartment SUVR} - 1) \times 100\%$. In addition, each lesion's distance to the nearest bone was calculated as the shortest Euclidean distance (mm) from the position of SUV_{max} on the PET image reconstructed with the 5-compartment attenuation map to the positions of the bone voxels on the 5-compartment attenuation map.

The 5-compartment attenuation maps were visually compared with the in-phase Dixon MR images, and bone registration errors near the lesion VOIs were reported. Since a substantial amount of bone registration errors were found near primary prostate tumors, we specifically evaluated the bias in ΔSUV in these regions; for each patient with bone registration errors near a primary tumor, 2 spheric VOIs of the same size were placed in prostate areas with and without misregistered bone, respectively. The SUV_{mean} was obtained for both VOIs, and ΔSUVs were calculated as described above.

The initial VOIs (before isocontouring) were delineated using OsiriX (20) (primary tumor VOIs) or ITK-SNAP (21) (all other VOIs). Subsequent isocontouring, SUV analysis, and calculation of distance to the nearest bone was performed in MATLAB 9.2 (The MathWorks Inc.).

Statistical Analysis

For the lesions without bone registration errors, linear mixed-effects models were used to test if ΔSUV and ΔSUVR were different from zero and to assess if ΔSUV and ΔSUVR were associated with the lesion's distance to the nearest bone. Furthermore, linear mixed-effects models were used to test if ΔSUV was different between lesions with and without bone registration errors. In all cases, patient number was used as a random effect on the intercept to account for multiple lesions per patient. The Wilcoxon signed-rank test was used to test if ΔSUV was different between prostate areas with and without misregistered bone. *P* values of less than 0.05 were considered significant. MATLAB 9.2 was used for statistical analysis.

RESULTS

The imaging data from 28 patients scanned between May 2014 and May 2015 as part of the staging study, and 81 patients scanned

between September 2015 and September 2016 as part of the recurrence study, were retrospectively analyzed. Twelve patients from the staging study were excluded from further analysis because of missing PET raw data ($n = 10$), complete failure of bone inclusion in the 5-compartment attenuation map ($n = 1$), or artifacts due to a hip prosthesis ($n = 1$). Fifty-eight patients from the recurrence study were excluded from further analysis because there were no PET findings ($n = 58$). In the remaining 39 patients ($n = 16$ for staging study, $n = 23$ for recurrence study), a total of 62 lesions was evaluated ($n = 28$ for staging study, $n = 34$ for recurrence study). The median prostate-specific antigen values were 16.7 ng/mL (range, 3.7–56.9 ng/mL) and 1.7 ng/mL (range, 0.2–12.3 ng/mL) for the patients from the staging and recurrence study, respectively.

Bone registration errors were found near 14 (64%) of 22 primary tumors (staging study), 1 (17%) of 6 pelvic lymph node metastases (staging study), 1 (13%) of 8 locally recurrent tumors (recurrence study), 2 (10%) of 21 pelvic lymph node metastases (recurrence study), 0 (0%) of 4 paraaortic lymph node metastases (recurrence study), and 1 (100%) of 1 bone metastases (recurrence study). Example cases are provided in Figure 1. $\Delta\text{SUV}_{\text{max}}$ and $\Delta\text{SUV}_{\text{iso}}$ were not significantly different between lesions with and without bone registration errors, neither for primary tumors alone ($P = 0.299$ and 0.282 , respectively) nor for all lesions combined ($P = 0.125$ and 0.241 , respectively). The largest increase in SUV was found for the bone lesion ($\Delta\text{SUV}_{\text{max}}$, 9.0%; $\Delta\text{SUV}_{\text{iso}}$, 8.8%), despite suboptimal coregistration of the bone atlas (Fig. 1D). In patients with bone registration errors near primary tumors, ΔSUV was significantly higher in prostate regions with than without misregistered bone ($P < 0.001$). The median bias in prostate regions with bone registration errors was +9.6 (range, 4.4–20.2) percentage point.

For the 43 lesions without artifacts, inclusion of bone in the attenuation map was associated with small but significant overall increases in SUV_{max} and SUV_{iso} ($\Delta\text{SUV}_{\text{max}}$, 2.5%; 95% confidence interval [CI], 2.0%–3.0%; $P < 0.001$) (SUV_{iso} , 2.5%; 95% CI, 1.9%–3.0%; $P < 0.001$). Figure 2A shows that the effect was similar for the prostate (bed) lesions ($n = 15$; $\Delta\text{SUV}_{\text{max}}$, 2.2%; 95% CI, 1.6%–2.9%; $P < 0.001$) ($\Delta\text{SUV}_{\text{iso}}$, 2.4%; 95% CI, 1.4%–3.3%; $P < 0.001$) and the lymph node lesions ($n = 28$; $\Delta\text{SUV}_{\text{max}}$, 2.6%; 95% CI, 1.9%–3.3%; $P < 0.001$) ($\Delta\text{SUV}_{\text{iso}}$, 2.5%; 95% CI, 1.8%–3.2%; $P < 0.001$). Neither $\Delta\text{SUV}_{\text{max}}$ ($P = 0.964$) nor $\Delta\text{SUV}_{\text{iso}}$ ($P = 0.620$) was associated with the lesion's distance to the nearest bone (Fig. 3A).

The inclusion of bone in the attenuation map was not associated with significant changes in SUVR_{max} or SUVR_{iso} when all lesions of the recurrence study were considered ($\Delta\text{SUVR}_{\text{max}}$, 0.2%; 95% CI, -0.5%–0.9%; $P = 0.604$) ($\Delta\text{SUVR}_{\text{iso}}$, 0.2%; 95% CI, -0.6%–1.0%; $P = 0.581$). Again, the results were comparable between prostate (bed) lesions ($\Delta\text{SUVR}_{\text{max}}$, 0.4%; 95% CI, -1.4%–2.1%; $P = 0.676$) ($\Delta\text{SUVR}_{\text{iso}}$, 0.8%; 95% CI, -1.8%–3.3%; $P = 0.562$) and lymph node lesions ($\Delta\text{SUVR}_{\text{max}}$, 0.1%; 95% CI, -0.7%–1.0%; $P = 0.737$) ($\Delta\text{SUVR}_{\text{iso}}$, 0.1%; 95% CI, -0.7%–0.9%; $P = 0.581$) (Fig. 2B), and no significant associations were found between $\Delta\text{SUVR}_{\text{max}}$ ($P = 0.982$) or $\Delta\text{SUVR}_{\text{iso}}$ ($P = 0.797$) and distance to bone (Fig. 3B).

DISCUSSION

Promising results from several studies with different radiopharmaceuticals indicate that PET/MRI has the potential to play an

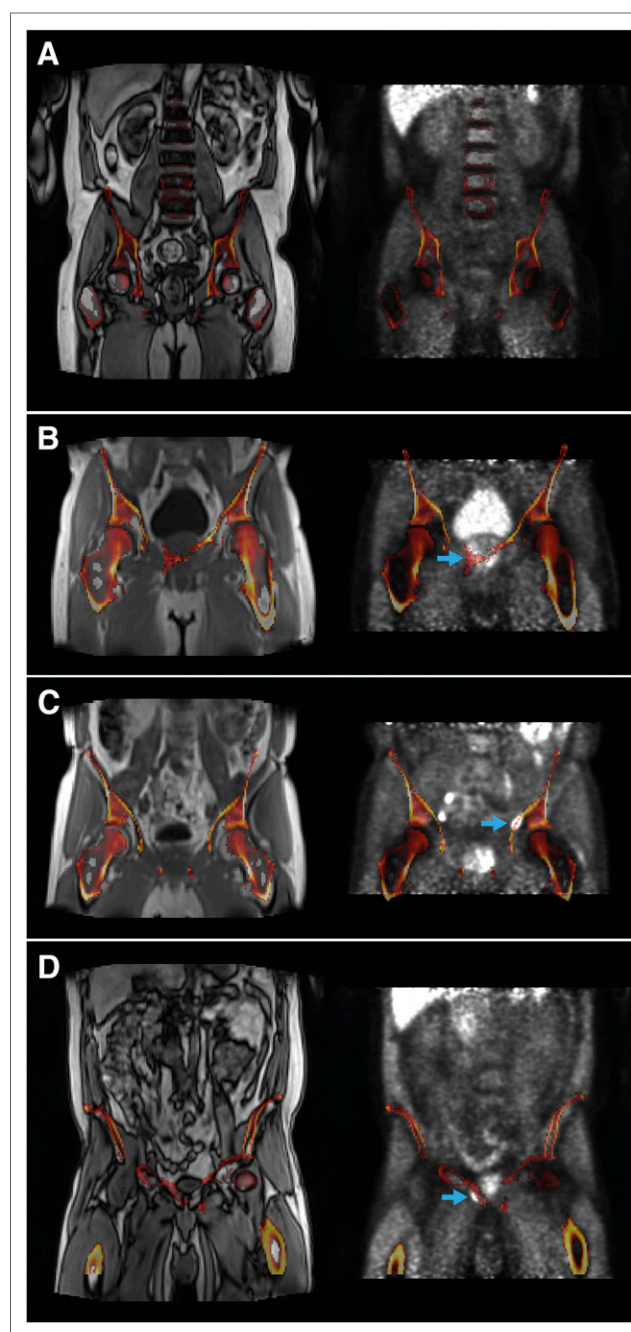


FIGURE 1. Coronal in-phase Dixon MR images (left) and PET images reconstructed with 4-compartment attenuation map (right) overlaid with 5-compartment attenuation map (linear attenuation coefficient $> 0.1 \text{ cm}^{-1}$, i.e., bone only) for case without bone registration errors (A) and cases with bone registration errors near primary tumor (B), pelvic lymph node metastasis (C), and bone lesion (D), as indicated by arrows

important role in staging of primary prostate cancer, for example (4,18,22,23), and detection of disease recurrence after initial treatment with curative intent, for example (24–27). However, in current clinical practice, the high linear attenuation coefficients of the bones in the pelvis and lower abdomen are assumed to be equal to those of soft tissue, which is incorrect. In this study, we applied a commercially available atlas-based method for including bone in the attenuation maps and evaluated its effect on the SUVs and

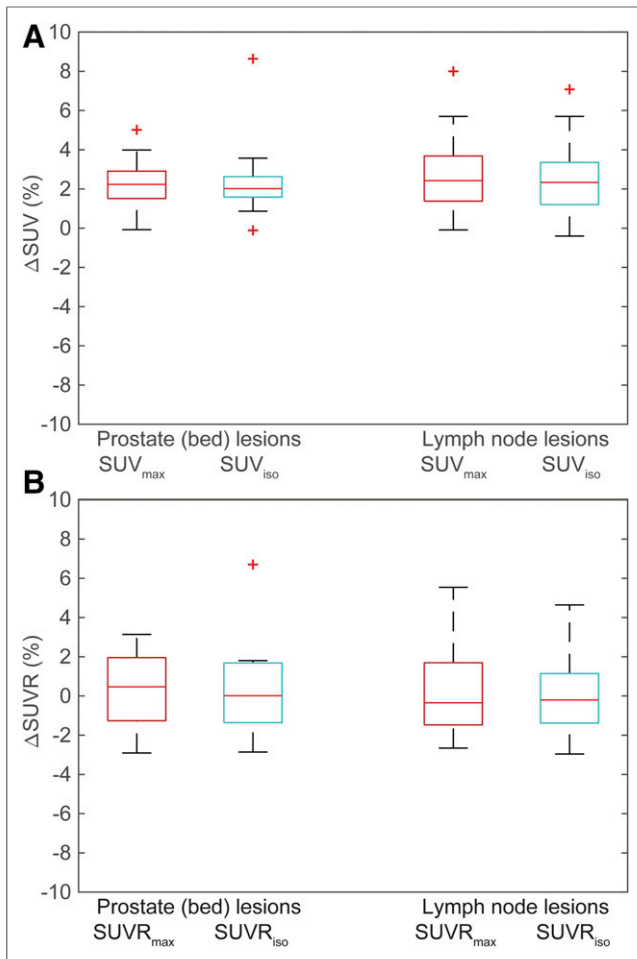


FIGURE 2. Box plots of relative difference in SUV (Δ SUV, A) and lesion-to-bone marrow SUVR (Δ SUVR, B) between PET images reconstructed with 4- and 5-compartment attenuation maps. Including bone in attenuation map was associated with significant increases in SUV_{max} and SUV_{iso} for both prostate (bed) and lymph node lesions. However, no significant changes were observed in SUV_{max} and SUV_{iso} .

SUVs of primary and recurrent prostate cancer lesions. We found that including bone resulted in significant but small increases in the SUV of prostate (bed) and lymph node lesions, which were on the order of 2%–3%. These results agree well with previously reported observed and simulated bias values from ignoring bone attenuation (11,13–15). We did not observe an effect of including bone attenuation on lesion-to-bone marrow SUVs, as the increases in SUV were similar for the lesion and bone marrow. Based on these results, and the bone registration errors discussed below, we deem the inclusion of bone in the PET/MRI attenuation maps not recommendable for the evaluation of soft-tissue prostate cancer lesions.

We found that bone registration errors may pose a problem in some patients, especially for prostate (bed) lesions when scanned in a single bed position. For the lesions analyzed in this study, the effect of including bone was not significantly different between lesions with and without bone registration errors. However, we did observe a significant bias in Δ SUV of approximately +10 percentage points when comparing prostate areas of the same patient with and without misregistered bone. These local inaccuracies could potentially misguide clinical decision making and need to be

resolved before we would advise this method for routine clinical prostate cancer imaging. Recently, acceleration techniques have been proposed that enable acquisition of higher-resolution Dixon images in the same scan time (28). In a study with 51 patients who underwent whole-body 18 F-FDG PET/MRI with high-resolution Dixon imaging, Oehmigen et al. did not observe any bone registration errors in the 5-compartment attenuation correction maps (15), which indicates that the higher level of anatomic detail in these images might lead to better results. High-resolution Dixon imaging was yet not available on our scanner when the data of this study were acquired; however, a direct comparison of pelvic bone registration errors in 5-compartment attenuation maps obtained from standard and high-resolution Dixon images is subject of future research.

A limitation of this study is that only one bone lesion was present in the evaluated patient cohort. Moreover, the lesion-containing bone was not correctly registered when included in the

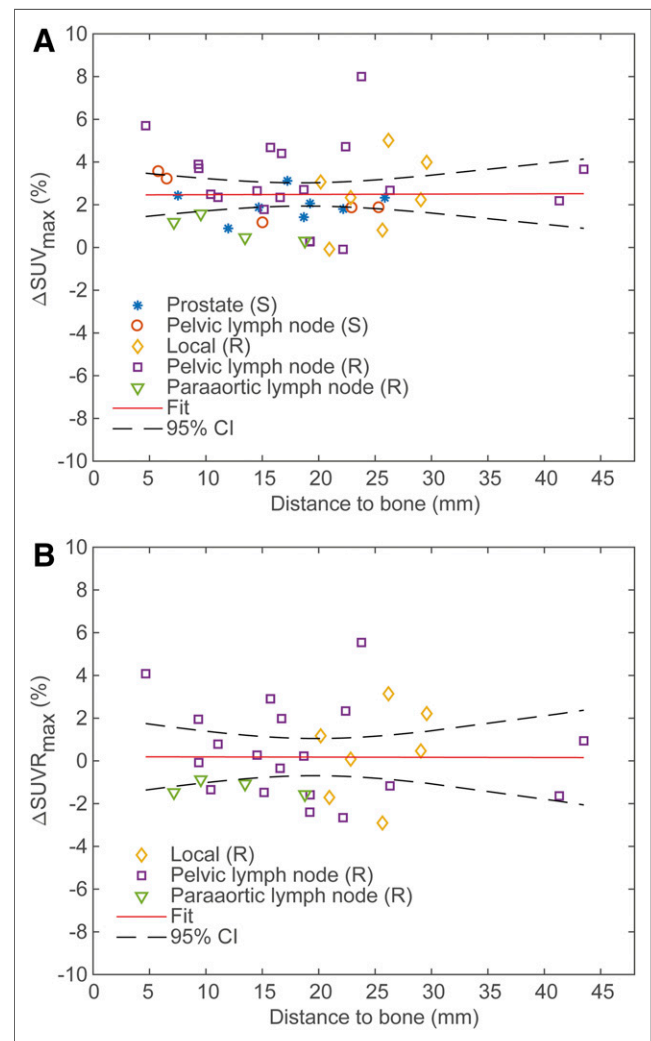


FIGURE 3. Plot showing relative difference in SUV_{max} (Δ SUV $_{max}$, A) and maximum lesion-to-bone marrow SUVR (Δ SUVR $_{max}$, B) between PET images reconstructed with 4- and 5-compartment attenuation maps, plotted as function of distance to nearest bone. Linear mixed-effects model analysis revealed that there were no significant associations between Δ SUV $_{max}$ or Δ SUVR $_{max}$ and distance to bone, as also illustrated by horizontal lines of model fits. (S) = staging study; (R) = recurrence study.

5-compartment attenuation map, which hampered proper comparison of SUVs between attenuation methods. Nevertheless, the relatively large increase in SUV observed for the bone lesion points toward a substantial effect of the attenuation correction method for this lesion type. Similar differences in bone lesion SUV between PET images reconstructed with the 4- and 5-compartment attenuation maps were found by others (14,15). Consequently, it would be recommendable to perform an additional reconstruction with a 5-compartment attenuation map when bone lesions are suspected based on the PET images reconstructed with the 4-compartment attenuation map.

Another limitation of this study is the lack of CT-based attenuation correction maps as a gold standard. Both the staging study and the recurrence study were PET/MRI only, so CT-derived attenuation maps of the same patients were not available for comparison. However, direct comparison between MRI and CT-derived attenuation correction is also challenging, as it is virtually impossible to keep the patient in the exact same position when scanned in a different scanner at a different time point. Our results are valuable because they show that atlas-based inclusion of bone in the attenuation maps is not likely to affect the clinical evaluation of soft-tissue lesions on ¹⁸F-fluciclovine PET/MR images of primary and recurrent prostate cancer, despite the high bone density of the pelvis. These results are in accordance with Oehmigen et al., who show that truncation of the arms is a larger source of SUV bias in the pelvis than ignoring bone (15). Whether our results are also valid for prostate cancer imaging with other PET radiopharmaceuticals, including prostate specific membrane antigen and choline-based tracers, remains to be seen and will be part of future research. In all cases, the atlas-based method may be important for the quantification of uptake in bone lesions, but the attenuation maps should always be checked for bone registration errors.

CONCLUSION

The investigated method for atlas-based inclusion of bone in Dixon-based attenuation correction of ¹⁸F-fluciclovine PET/MRI has only a small effect on the SUVs of soft-tissue prostate cancer lesions, and no effect on their lesion-to-bone marrow SUVs when using signal from L3 as a reference. The attenuation maps should always be checked for bone registration errors when evaluating lesions in or close to the bones.

DISCLOSURE

This study was funded by The Norwegian Cancer Society and the Movember Foundation (grants 100792 and 102050). No other potential conflict of interest relevant to this article was reported.

REFERENCES

- Torre LA, Bray F, Siegel RL, Ferlay J, Lortet-Tieulent J, Jemal A. Global cancer statistics, 2012. *CA Cancer J Clin*. 2015;65:87–108.
- Barentsz JO, Weinreb JC, Verma S, et al. Synopsis of the PI-RADS v2 guidelines for multiparametric prostate magnetic resonance imaging and recommendations for use. *Eur Urol*. 2016;69:41–49.
- Turkbey B, Mena E, Shih J, et al. Localized prostate cancer detection with ¹⁸F-FACBC PET/CT: comparison with MR imaging and histopathologic analysis. *Radiology*. 2014;270:849–856.
- Eiber M, Weirich G, Holzapfel K, et al. Simultaneous ⁶⁸Ga-PSMA HBED-CC PET/MRI improves the localization of primary prostate cancer. *Eur Urol*. 2016;70:829–836.
- Schuster DM, Nieh PT, Jani AB, et al. Anti-3-[¹⁸F]FACBC positron emission tomography-computerized tomography and ¹¹¹In-capromab pendetide single photon emission computerized tomography-computerized tomography for recurrent prostate carcinoma: results of a prospective clinical trial. *J Urol*. 2014;191:1446–1453.
- Eiber M, Maurer T, Souvatzoglou M, et al. Evaluation of hybrid ⁶⁸Ga-PSMA ligand PET/CT in 248 patients with biochemical recurrence after radical prostatectomy. *J Nucl Med*. 2015;56:668–674.
- Afshar-Oromieh A, Holland-Letz T, Giesel FL, et al. Diagnostic performance of ⁶⁸Ga-PSMA-11 (HBED-CC) PET/CT in patients with recurrent prostate cancer: evaluation in 1007 patients. *Eur J Nucl Med Mol Imaging*. 2017;44:1258–1268.
- Elschot M, Selnaes KM, Sandsmark E, et al. Combined ¹⁸F-fluciclovine PET/MRI shows potential for detection and characterization of high-risk prostate cancer. *J Nucl Med*. 2018;59:762–768.
- Afshar-Oromieh A, Haberkorn U, Schlemmer HP, et al. Comparison of PET/CT and PET/MRI hybrid systems using a ⁶⁸Ga-labelled PSMA ligand for the diagnosis of recurrent prostate cancer: initial experience. *Eur J Nucl Med Mol Imaging*. 2014;41:887–897.
- Schulz V, Torres-Espallardo I, Renisch S, et al. Automatic, three-segment, MR-based attenuation correction for whole-body PET/MR data. *Eur J Nucl Med Mol Imaging*. 2011;38:138–152.
- Martinez-Möller A, Souvatzoglou M, Delso G, et al. Tissue classification as a potential approach for attenuation correction in whole-body PET/MRI: evaluation with PET/CT data. *J Nucl Med*. 2009;50:520–526.
- Aznar MC, Sersar R, Saabye J, et al. Whole-body PET/MRI: the effect of bone attenuation during MR-based attenuation correction in oncology imaging. *Eur J Radiol*. 2014;83:1177–1183.
- Keereman V, Holen RV, Mollet P, Vandenberghe S. The effect of errors in segmented attenuation maps on PET quantification. *Med Phys*. 2011;38:6010–6019.
- Paulus DH, Quick HH, Geppert C, et al. Whole-body PET/MR imaging: quantitative evaluation of a novel model-based MR attenuation correction method including bone. *J Nucl Med*. 2015;56:1061–1066.
- Oehmigen M, Lindemann ME, Gratz M, et al. Impact of improved attenuation correction featuring a bone atlas and truncation correction on PET quantification in whole-body PET/MR. *Eur J Nucl Med Mol Imaging*. 2018;45:642–653.
- Koesters T, Friedman KP, Fenchel M, et al. Dixon sequence with superimposed model-based bone compartment provides highly accurate PET/MR attenuation correction of the brain. *J Nucl Med*. 2016;57:918–924.
- Miller MP, Kostakoglu L, Pryma D, et al. Reader training for the restaging of biochemically recurrent prostate cancer using ¹⁸F-fluciclovine PET/CT. *J Nucl Med*. 2017;58:1596–1602.
- Selnaes KM, Krüger-Stokke B, Elschot M, et al. ¹⁸F-fluciclovine PET/MRI for preoperative lymph node staging in high-risk prostate cancer patients. *Eur Radiol*. 2018;28:3151–3159.
- Elschot M, Selnaes KM, Sandsmark E, et al. A PET/MRI study towards finding the optimal [¹⁸F]fluciclovine PET protocol for detection and characterisation of primary prostate cancer. *Eur J Nucl Med Mol Imaging*. 2017;44:695–703.
- Rosset A, Spadola L, Ratib O. OsiriX: an open-source software for navigating in multidimensional DICOM images. *J Digit Imaging*. 2004;17:205–216.
- Yushkevich PA, Piven J, Hazlett HC, et al. User-guided 3D active contour segmentation of anatomical structures: significantly improved efficiency and reliability. *Neuroimage*. 2006;31:1116–1128.
- Jambor I, Kuisma A, Kahkonen E, et al. Prospective evaluation of ¹⁸F-FACBC PET/CT and PET/MRI versus multiparametric MRI in intermediate- to high-risk prostate cancer patients (FLUCIPRO trial). *Eur J Nucl Med Mol Imaging*. 2018;45:355–364.
- Piert M, Montgomery J, Kunju LP, et al. ¹⁸F-choline PET/MRI: the additional value of PET for MRI-guided transrectal prostate biopsies. *J Nucl Med*. 2016;57:1065–1070.
- Grubmüller B, Baltzer P, D'Andrea D, et al. ⁶⁸Ga-PSMA 11 ligand PET imaging in patients with biochemical recurrence after radical prostatectomy: diagnostic performance and impact on therapeutic decision-making. *Eur J Nucl Med Mol Imaging*. 2018;45:235–242.
- Kranzbühler B, Nagel H, Becker AS, et al. Clinical performance of ⁶⁸Ga-PSMA-11 PET/MRI for the detection of recurrent prostate cancer following radical prostatectomy. *Eur J Nucl Med Mol Imaging*. 2018;45:20–30.
- Freitag MT, Radtke JP, Afshar-Oromieh A, et al. Local recurrence of prostate cancer after radical prostatectomy is at risk to be missed in ⁶⁸Ga-PSMA-11-PET of PET/CT and PET/MRI: comparison with mpMRI integrated in simultaneous PET/MRI. *Eur J Nucl Med Mol Imaging*. 2017;44:776–787.
- Minamimoto R, Sonni I, Hancock S, et al. Prospective evaluation of ⁶⁸Ga-RM2 PET/MRI in patients with biochemical recurrence of prostate cancer and negative conventional imaging. *J Nucl Med*. 2018;59:803–808.
- Freitag MT, Fenchel M, Baumer P, et al. Improved clinical workflow for simultaneous whole-body PET/MRI using high-resolution CAIPRINHA-accelerated MR-based attenuation correction. *Eur J Radiol*. 2017;96:12–20.